



Wave-Structure Interaction (WSI) Analysis for Dam Break with Dike using SPH and ALE Methods

Ahmad Rahmati Alaei^{1*}, Hamid Rokhy²

¹ Assistant professor, Department of Mechanical Engineering, National University of Skills (NUS), Tehran, Iran. Email: arahmatialaei@nus.ac.ir, ORCID: [0000-0002-7681-230X](https://orcid.org/0000-0002-7681-230X)

² Amir Kabir University of Technology, Department of Aerospace Engineering, Tehran, Iran. Email: h.rokhy@gmail.com, <https://orcid.org/0000-0002-4827-7346>

* Corresponding author: Ahmad Rahmati Alaei: arahmatialaei@nus.ac.ir

Received: 08/10/2024

Revised: 02/03/2025

Accepted: 18/03/2025

ABSTRACT: Dams break when their gates are suddenly removed, allowing fluid to flow instantly and causing deaths and massive damage. In addition, tsunamis can damage coastal structures. This research employs smoothed particle hydrodynamics (SPH) and arbitrary Lagrangian-Eulerian (ALE) formulations to address wave–structure interaction (WSI) problems. This study employs a weakly compressible equation of state (EOS), specifically the Murnaghan EOS, to reduce fluid compressibility and impose acceptable numerical timestep constraints using LS-DYNA. The numerical results for wave forces on the obstacle are accurately validated against experimental data. The SPH method demonstrates better agreement with experimental results compared to the ALE method. A mesh sensitivity analysis is conducted for both methods, and appropriate element sizes and particle numbers are selected for the SPH and ALE methods, respectively. The study investigates how dike height and obstacle distance impact fluid wave reduction. Comparing the H5D15 model ($F_{max} = 13.4 N$) and H10D45 model ($F_{max} = 7.5 N$) shows that increasing dike height is more effective than reducing the barrier distance. Longitudinal expansion decreases fluid force by 28% (to $9.8 N$), while transverse expansion reduces it by 33% (from $13.6 N$ to $9.2 N$), with transverse variations being more effective in lowering hydrodynamic wave forces.

Keywords: Wave-Structure Interaction (WSI), Dam Break, Smoothed Particle Hydrodynamics (SPH), Arbitrary Lagrangian-Eulerian (ALE), Dike.

1. Introduction

A dam break refers to the uncontrolled, instantaneous release of fluid from a stationary state due to the sudden removal of a barrier, often resulting in significant loss of life and substantial economic damage. Additionally, tsunami-induced coastal waves can have devastating effects on structures. The smoothed particle hydrodynamics (SPH) and arbitrary Lagrangian-Eulerian (ALE) methods have proven to be reliable and efficient numerical tools for addressing wave–structure interaction (WSI) problems, which are prevalent in dam break and coastal wave phenomena. In recent years, both methods have seen significant improvements in accuracy and efficiency, garnering considerable attention from researchers in the field of computational fluid dynamics (CFD) (Wu et al., 2022; Xie et al., 2023; Cai et al., 2021; Jacob et al., 2021).

The SPH method is a purely Lagrangian approach that approximates the governing partial differential equations (PDEs) of a problem using particle kernel approximation, unlike mesh-based numerical methods. This method is applicable to both compressible and incompressible fluids and offers several advantages over traditional mesh-based approaches such as the finite difference method (FDM) and finite element method (FEM). For instance, SPH inherently handles advection accurately for complex geometries without requiring interface tracking or adaptive meshing (Pozorski & Olejnik, 2024). However, accurately modeling wall behavior remains a challenge in SPH. Preventing particle penetration under no-slip and partial-slip conditions is an ongoing issue in the development of SPH methods. Furthermore, the method's high computational cost and time requirements, particularly for three-dimensional problems requiring a large number of particles, are notable limitations (Nishiura et al., 2015).

The ALE approach is one of the most widely used methods for simulating fluids with large motions, such as sloshing in tanks. This method combines the advantages of both Lagrangian and Eulerian frameworks, allowing computational domain nodes to move with the material (Lagrangian), remain fixed (Eulerian), or move arbitrarily (Ozdemir et al., 2009). In recent years, researchers have developed numerous computational models to analyze water-sediment interaction (WSI) using both SPH and ALE methods (Wang & Chang, 2025; Wu & Garlock, 2024; Torabbeigi et al., 2024; Altomare et al., 2023; Chang & Wu, 2023; Han & Dong, 2022). Salis et al. (2024) developed a 3D SPH-based computational model to predict wave profiles, impact forces, and structural dynamics of floating structures. Liu et al. (2013) introduced a 2D incompressible SPH (ISPH) model to study free-surface flow interactions with structures, employing an enhanced mirror particle approach for solid boundary treatment. The model was validated for wave interactions with coastal structures of various shapes. Using the DualSPHysics code, Altomare et al. (2020) modeled a real-world engineering test case for WSI during Storm Gloria.

Crespo et al. (2015) developed SPHYSICS, an open-source SPH code, to investigate free-surface flow phenomena, including wave and dam-break effects on offshore structures. SPHYSICS was used to study the impact of a single wave on a tall coastal structure (Gómez-Gesteira et al., 2012) with numerical results for velocities and forces showing excellent agreement with experimental data. Domínguez et al. (2019) also utilized this open-source code to simulate WSI problems for floating offshore constructions, both freely moving and tethered to the seabed. Their numerical models were validated against experimental data for free-surface elevation, floating motion, and mooring tensions. Using the Color Domain Particle (CDP)

technique, Ren et al. (2018) developed a 2D weakly compressible SPH (WCSPH) model to study wave-thin structure interactions.

Lou & Jin (2014) employed an ALE approach to simulate solitary waves and run-up waves interacting with elastic breakwaters and drifting objects. They conducted comprehensive simulations of solitary wave impacts and drifting object collisions using LS-DYNA. For fluid-structure interaction (FSI) problems, Basting et al. (2017) proposed an extended ALE method incorporating a variational mesh optimization technique. This method maintains mesh connectivity and alignment with the structure, even under large structural displacements.

Bai et al. (2020) modeled free-surface wave tracking in a tank using the ALE method and the Navier-Stokes solver in OpenFOAM®. Their study focused on an internal mass wavemaking method with ALE surface-tracking technology, rather than the traditional volume-of-fluid (VOF) scheme. Xu et al. (2015) simulated sloshing in a half-filled tank using both ALE and SPH formulations. They concluded that the particle spacing in the SPH method should be at least twice as fine as the ALE mesh to achieve comparable accuracy. Rezaiee-Pajand et al. (2024) introduces a new approach for modal analysis of dam-reservoir systems using two cubic eigenvalue problems. This method, referred to as the cubic ideal-coupled approach, improves upon the decoupled and ideal-coupled methods, offering greater accuracy in the dynamic analysis of concrete gravity dams.

The primary objective of this study is to develop the SPH and ALE methods for solving WSI problems using LS-DYNA commercial code. DualSPHysics code (Crespo et al., 2015) is optimized for SPH but lacks native support for FEM or ALE, limiting its use in fluid-structure systems. LS-DYNA, however, seamlessly integrates SPH with ALE and FEM for comprehensive simulations of fluid dynamics and structural behavior, while also offering superior computational scalability for large-scale applications. This paper presents 3D SPH and ALE models to simulate the WSI problem involving large waves generated by dam breaks impacting tall coastal structures. The wave forces acting on the structure show excellent agreement with experimental data. Furthermore, the effectiveness of dikes in mitigating fluid waves is investigated.

2. Numerical Approaches

Various formulations, such as the ALE and SPH methods, have been employed for wave-structure interaction (WSI) analysis. This section provides a detailed description of the ALE and SPH formulations applied to WSI problems.

2.1. Smoothed Particle Hydrodynamics (SPH)

SPH is a modern numerical method for modeling fluid behavior. Unlike conventional Computational Fluid Dynamics (CFD) techniques, SPH's most significant advantage lies in its mesh-free particle (MFP) approach. In this method, a system's movement and state are represented using a finite set of discrete particles. SPH is fundamentally an interpolation-based technique, making it particularly suitable for problems involving large deformations, such as wave-structure interaction (WSI), where significant element distortion is anticipated. The interpolation integral for any quantity $A(\mathbf{r})$ over the domain Ω is defined as follows (Kelager, 2006; Sunara et al., 2021):

$$A(\vec{r}) = \int_{\Omega} A(\vec{r}')W(\mathbf{r} - \vec{r}', h)d\vec{r}' \quad (1)$$

where W , \mathbf{r} , \mathbf{r}' , and h represent the kernel function, the position of the particle, the position of the neighboring particle, and the smoothing length (or core radius), respectively.

As illustrated in Figure 1, the approximation of $A(\mathbf{r})$ for a particle "a" in discrete form is expressed as:

$$A(\mathbf{r}_a) = \sum_b m_b \frac{A_b}{\rho_b} W(\mathbf{r}_b - \mathbf{r}_a, h) \quad (2)$$

where m_b and ρ_b represent the mass and density of particle "b", respectively.

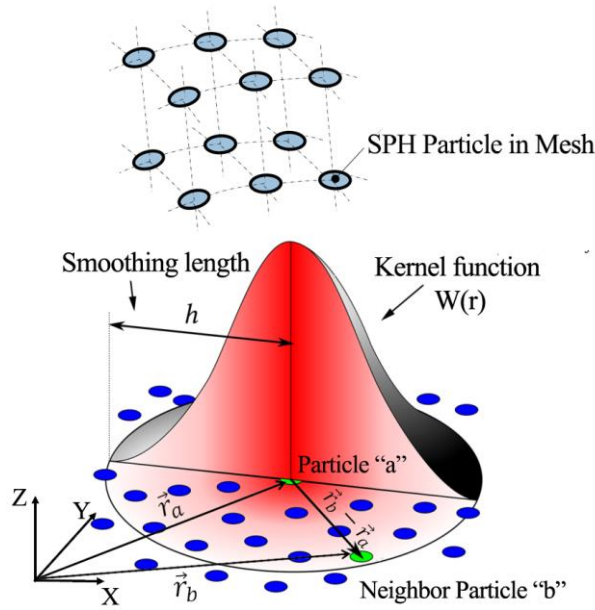


Figure 1. SPH approximation for particle

The kernel function must satisfy several requirements, including positivity, compact support, and normalization. Additionally, it should monotonically decrease as the distance from the particle increases and behave like a delta function as the smoothing length approaches zero. The kernel-based cubic spline function is defined as:

$$W(\mathbf{r}_b - \mathbf{r}_a, h) = \frac{1}{\pi h^3} \begin{cases} 1 - \frac{3}{2}q^2 + \frac{3}{4}q^3 & \text{if } 0 \leq q \leq 1 \\ \frac{1}{4}(2 - q)^3 & \text{if } 1 \leq q \leq 2 \\ 0 & \text{if } q \geq 2 \end{cases} \quad (3)$$

where $\mathbf{q} = \mathbf{r}/h$ and \mathbf{r} are the distance between particles.

Obviously, the accuracy of the SPH results significantly depends on the selection of the kernel function

2.1.1. Momentum Conservation Equation

The momentum conservation equation for fluid dynamics in the SPH method is:

$$\frac{\partial \mathbf{v}}{\partial t} = \sum_b m_b \left(\frac{P_b}{\rho_b^2} + \frac{P_a}{\rho_a^2} + \Pi_{ab} \right) \vec{\nabla} W_{ab} + \mathbf{g} \quad (4)$$

where g is the acceleration of gravity; P_a, ρ_a, P_b, ρ_b are pressures and densities corresponding to particles "a" and "b"; Π_{ab} is the viscosity term as bellow:

$$\Pi_{ab} = \begin{cases} \frac{-\alpha \bar{c}_{ab} \mu_{ab}}{\bar{\rho}_{ab}} & \mathbf{v}_{ab} \cdot \mathbf{r}_{ab} < 0 \\ 0 & \mathbf{v}_{ab} \cdot \mathbf{r}_{ab} > 0 \end{cases} \quad (5)$$

$$\mu_{ab} = \frac{h \mathbf{v}_{ab} \cdot \mathbf{r}_{ab}}{\mathbf{r}_{ab}^2 + 0.01 h^2} \quad (6)$$

$$\bar{c}_{ab} = \frac{c_a + c_b}{2} \quad (7)$$

$$\bar{\rho}_{ab} = \frac{\rho_a + \rho_b}{2} \quad (8)$$

where $\alpha = 0.1$, $\mathbf{r}_{ab} = \mathbf{r}_a - \mathbf{r}_b$ and $\mathbf{v}_{ab} = \mathbf{v}_a - \mathbf{v}_b$. In addition $c_a, c_b, \mathbf{r}_a, \mathbf{r}_b, \mathbf{v}_a, \mathbf{v}_b$ are sound speed, position, and velocity of particle "a" or "b", respectively.

2.1.2. Continuity Equation

Changes in fluid density are calculated through the continuity equation as follows:

$$\frac{\partial \rho}{\partial t} = \sum_b m_b \mathbf{v}_{ab} \cdot \vec{\nabla} W_{ab} \quad (9)$$

2.2. Arbitrary Lagrangian-Eulerian (ALE)

The ALE method is a computational approach used in finite element numerical analysis (FEA). In this method, the grid of elements in the space of interest is neither fixed (Eulerian approach) nor rigidly connected to the material (Lagrangian approach); instead, the mesh of elements and the material have relative motion. This method is an efficient tool for modeling problems such as WSI, where large and intense local deformations occur in the material.

In the ALE method, the transfer effects caused by the relative movement between the mesh and the material are expressed as:

$$\frac{\partial f(X_i, t)}{\partial t} = \frac{\partial f(x_i, t)}{\partial t} + w_i \frac{\partial f(x_i, t)}{\partial x_i} \quad (10)$$

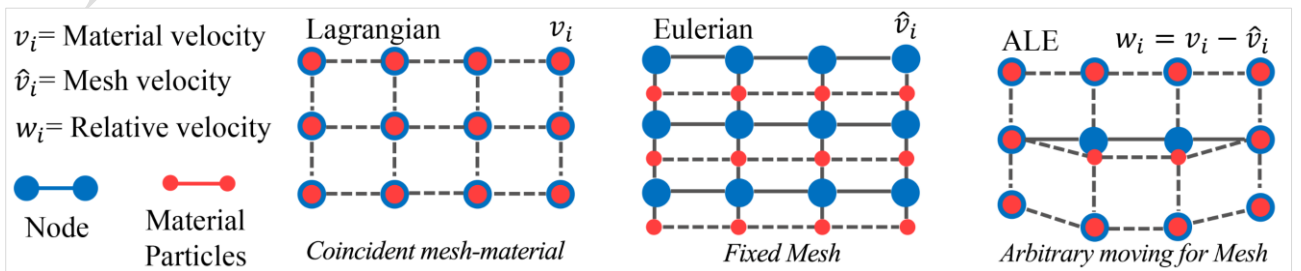


Figure 2. Lagrangian, Eulerian, and ALE approaches

where X_i, x_i and $w_i = v_i - \hat{v}_i$ are the Lagrangian coordinate, Eulerian coordinate, and relative velocity between the material and mesh, respectively. The last term in the equation (10) represents the transfer effects caused by the relative movement between the mesh and the material.

As shown in Figure 2, the mesh and the material connect when their velocities are equal ($v_i = \hat{v}_i$), forming the Lagrangian approach. If the mesh is fixed ($\hat{v}_i = 0$), this represents the Eulerian method. When the mesh moves at a different velocity relative to the material ($v_i \neq \hat{v}_i$), the ALE method is used. Therefore, the following conservation equations provide the governing equations for the ALE formulation:

2.2.1. Mass Equation:

$$\frac{\partial \rho}{\partial t} = -\rho \frac{\partial v_i}{\partial x_i} - w_i \frac{\partial \rho}{\partial x_i} \quad (11)$$

2.2.2. Momentum equation:

$$\rho \frac{\partial v_i}{\partial t} = \sigma_{ij,j} + \rho b_i - \rho w_i \frac{\partial v_i}{\partial x_j} \quad (12)$$

where $\sigma_{ij,j}, b_i$ are the Cauchy stress tensor and body force vector, respectively.

LS-DYNA is a well-known commercial engineering software that employs the SPH and ALE numerical methods. This code can simulate WSI problems by combining the finite element method (FEM) and the SPH approach.

3. Experimental Setup

The experimental setup for the WSI problem (Figure 3) consists of a container with dimensions of 1.6 m × 0.61 m × 0.75 m. The initial volume of water behind the gate is 0.4 m (length) × 0.61 m (width) × 0.3 m (height). Following the test conditions outlined by (Gómez-Gesteira et al., 2012), a thin layer of water with a height of approximately 0.01 m is considered at the bottom of the container. The obstacle, with dimensions of 0.12 m × 0.12 m × 0.75 m, is located downstream of the gate and in the center of the water domain.

Table 1. Numerical model components

	Water	Obstacle (Column)
Material model	*Null	*Rigid
EOS	*MURNAGHAN	-
Material parameters	$\rho = 1000 \text{ kg/m}^3$ $P_c = -5 \times 10^4 \text{ Pa}$ $MU = 0.001$	$\rho = 100 \text{ kg/m}^3$ $E = 2 \times 10^4 \text{ Pa}$ $\vartheta = 0.25$
EOS parameters	$\gamma = 7$ $k_0 = 1.5 \times 10^5$	-
Element type	SPH: Particles ALE: Solid (Hex: CST)	Solid (Hex: CST)
Number of elements (particles)	SPH: 683394 ALE: 79056	11700

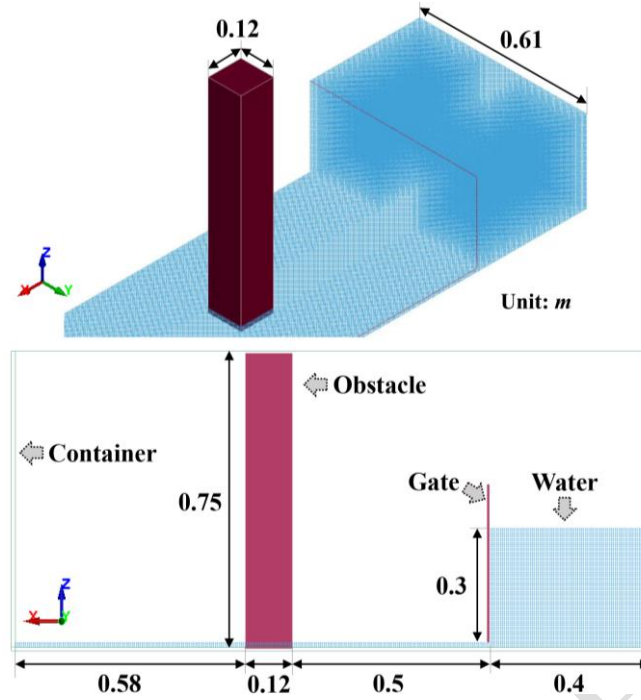


Figure 3. Experimental setup for WSI problem

Experimentally, the net force exerted on the structure and the fluid velocities at different locations were recorded.

4. Numerical Model

As shown in Figure. 4, this paper simulates the WSI using two numerical approaches, ALE and SPH, within the robust finite element analysis code LS-DYNA.

4.1. Constitutive Material Models

Table 1 specifies material models and their coefficients for numerical model components, including water and obstacles, in both SPH and ALE simulation methods. The obstacle column with a square cross-section is considered rigid. In the SPH and ALE models, the number of particles and fluid elements are 683,394 and 79,056, respectively. The material model *MAT_Null, which characterizes the density and viscosity of the fluid, is employed alongside an equation of state (EOS) necessary for the pressure-density relationship.

4.2. MURNAGHAN EOS

To minimize fluid compressibility and ensure suitable timestep limitations, a weakly compressible EOS is used. With an acceptable explicit calculation timestep, the Murnaghan EOS (Yreux, 2018) enforces quasi-incompressibility. The pressure is defined as:

$$p = k_0 \left[\left(\frac{\rho}{\rho_0} \right)^\gamma - 1 \right] \quad (13)$$

where ρ_0 is the fluid's density at rest, γ is a number that is usually set to 7, and k_0 is chosen so that:

$$c_0 = \sqrt{\frac{\gamma k_0}{\rho_0}} \geq 10v_{max} \quad (14)$$

where v_{max} is the maximum fluid flow velocity that is predicted.

4.3. Contacts & Interactions

The AUTOMATIC_NODE_TO_SURFACE contact algorithm is adopted for the SPH model, employing a penalty-type formulation to simulate the interaction between the fluid and the obstacle. In penalty-based contact, the contact force is computed as proportional to the penetration depth, the extent of constraint violation, and the numerical stiffness value.

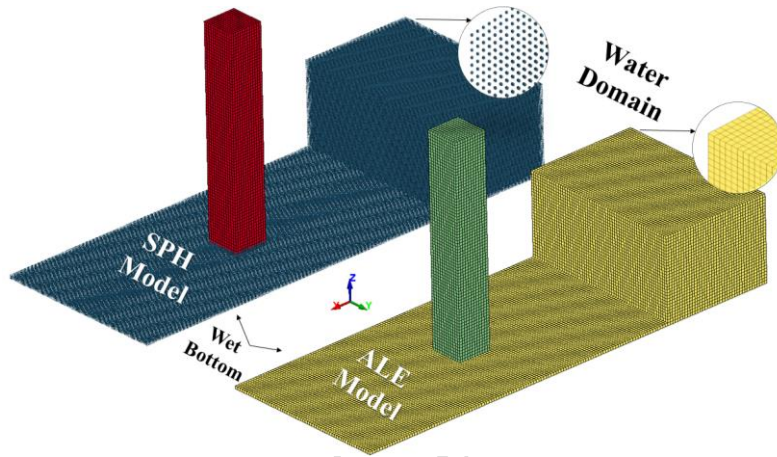


Figure 4. SPH and ALE numerical model

Penalty coupling functions similarly to a spring system, calculating the penalty forces based on the penetration depth and spring stiffness. Figure 5 illustrates the connection of the spring's head to the slave node and its tail to the master node within a fluid particle. In the ALE approach, the *CONSTRAINED_LAGRANGE_IN_SOLID keyword is utilized to account for the interaction between the fluid and the obstruction.

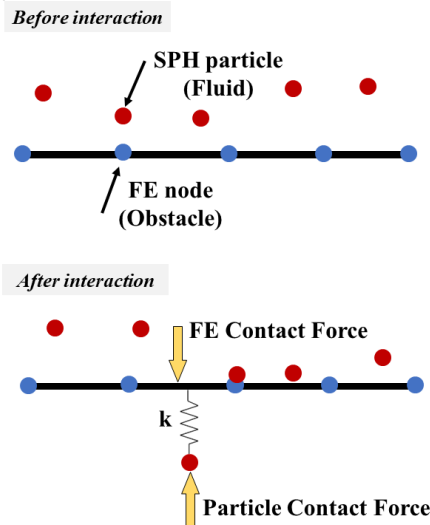


Figure 5. SPH-FE penalty contact for fluid and obstacle

5. Result and Discussion

5.1. Mesh Sensitivity Analysis

To analyze the fluid mesh's sensitivity, the SPH and ALE methods use different element sizes and particle counts, respectively: 2 cm, 1 cm, and 0.5 cm elements, as well as 14,737, 90,717, and 683,394 particles.

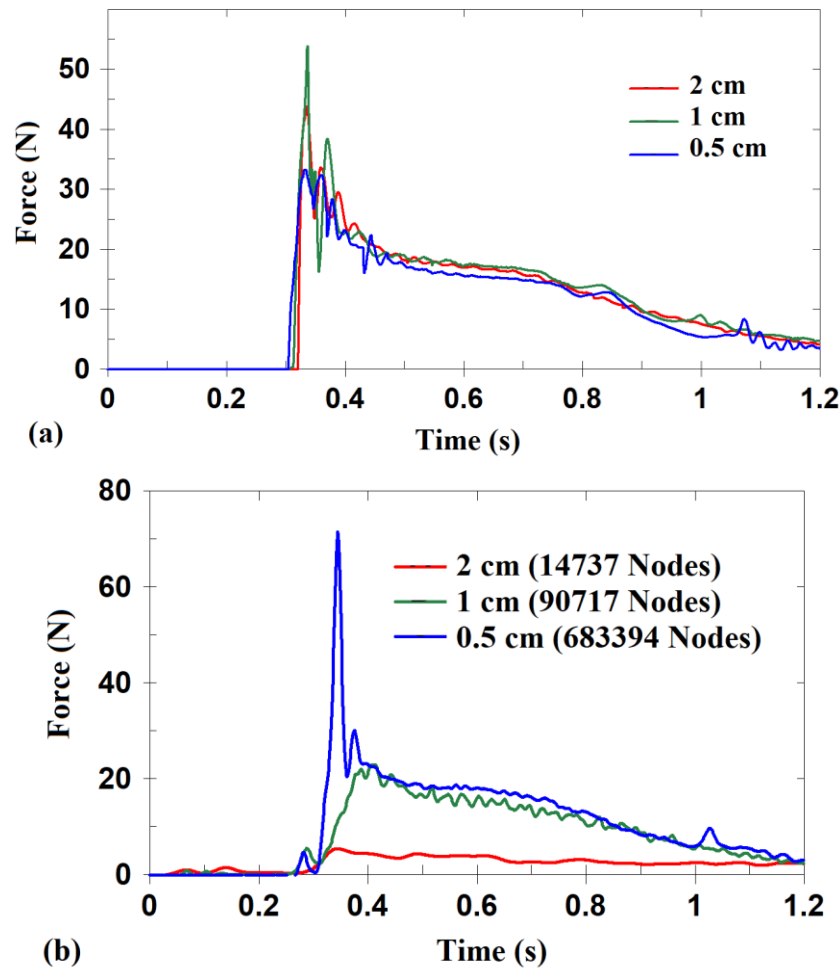
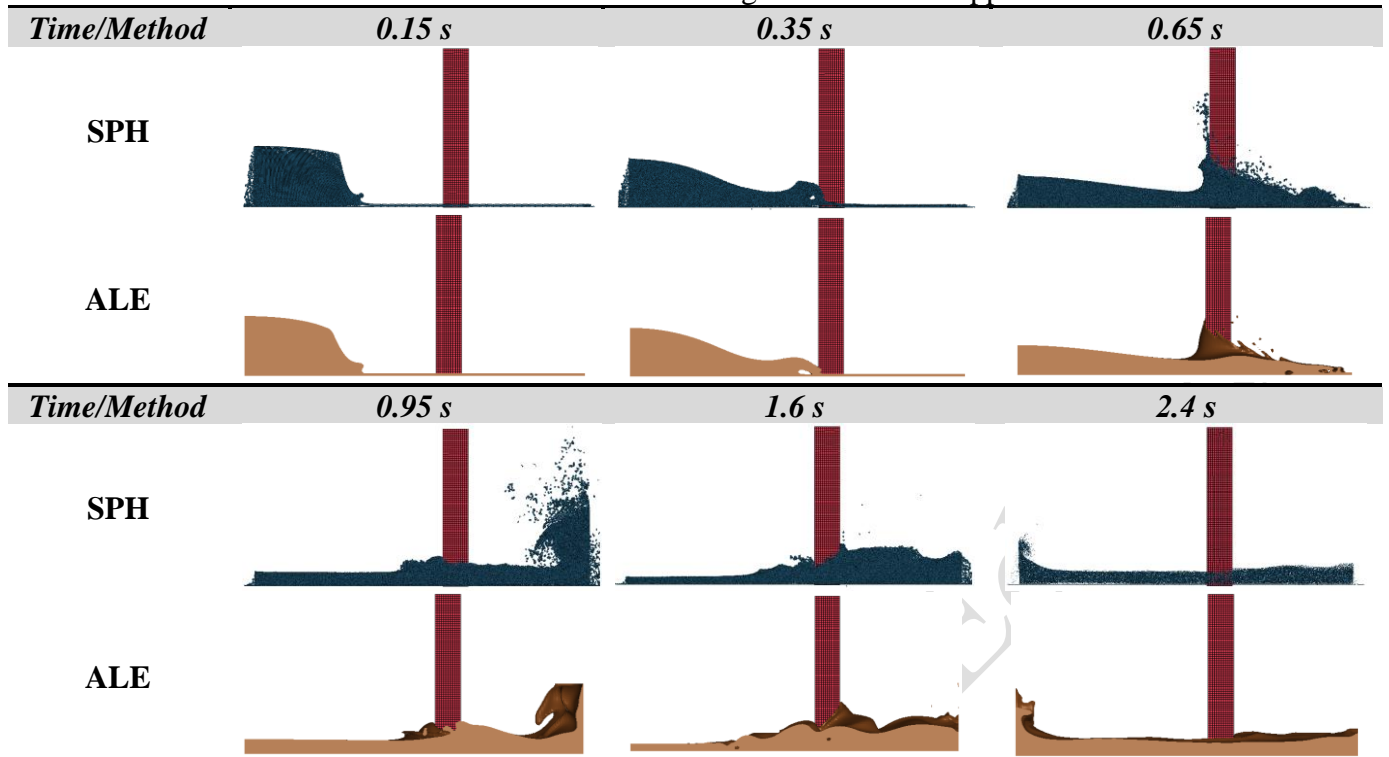


Figure 6. Fluid mesh sensitivity; (a) ALE, (b) SPH

Figure 6 shows the mesh sensitivity analysis for the SPH and ALE methods. As observed, under the three element size conditions, the changes in the force applied to the rigid obstacle in the ALE analysis are closely aligned (Figure 6-a). As the number of particles in the SPH analysis increased, the results for models with 90,717 and 683,394 particles converged (Figure 6-b). To save computational time and cost while maintaining acceptable accuracy, an element size of 1 cm and 683,394 particles are selected for the ALE and SPH numerical models, respectively.

Table 2. Fluid wave evolution using SPH and ALE approaches



5.2. Validation of Numerical Model

Table 2 compares the fluid wave evolution and its collision with the obstacle at various time points using both the SPH and ALE methods. The travelling wave impacts the solid barrier at approximately 0.35 s, reaches the container's face at 0.65 s, and subsequently forms a return wave. The fluid reaches a stable state after 2.4 s. Figure 7 shows the force exerted on the obstacle as determined by SPH, ALE, and experimental results. A clear correlation exists between the experimental and numerical values. A slight difference is observed in the peak value compared to the experimental results, likely due to the relatively lower accuracy reported in the experimental data (Gómez-Gesteira et al., 2012)

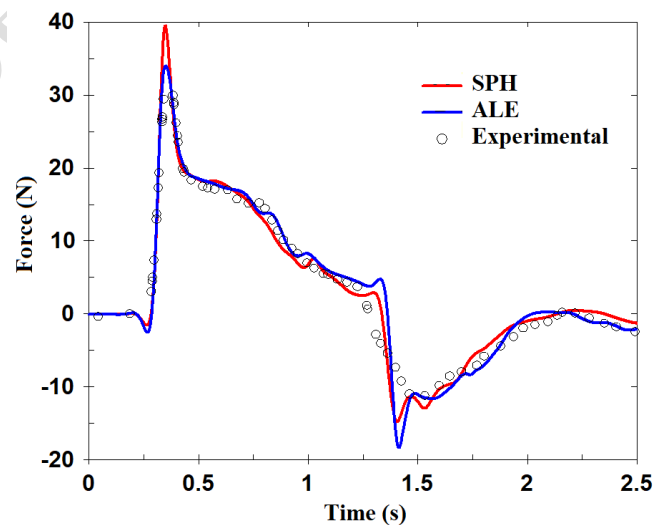


Figure 7. Wave force on obstacle, comparison for numerical and experimental result

Table 3. Parametric study for dike effect

Model	Method	D (cm)	H (cm)	Length	Width	F _{max} (N)
SPH01	SPH					39.9
ALE01	ALE	No Dike	No Dike			34
Test01	Experiment					38
H5D15		15				13.4
H5D30		30	5			22.8
H5D45		45		12	12	24.4
H10D15						
L12-H10D15		15				7.15
W12-H10D15						
H10D30	SPH	30	10			12
H10D45		45				20.8
L24-H10D15				24	12	9.8
L36-H10D15				36	12	10.1
W24-H10D15		15	10	12	24	9.2
W36-H10D15				12	36	12.7

Based on Figure 7, the SPH method provides a response closer to the experimental data compared to the ALE method, particularly regarding the minimum and maximum values. Therefore, we selected the SPH method for the parametric study in the following sections.

5.3. Dike Effect on Wave Mitigation

This section analyzes how dikes mitigate the impact of large waves on coastal structures. The distance of the dike from the obstacle (D) and the height of the dike (H) are the key parameters controlling the wave reduction process. In general, the force increases as the height of the dike decreases and the distance between the dike and the rigid barrier increases.

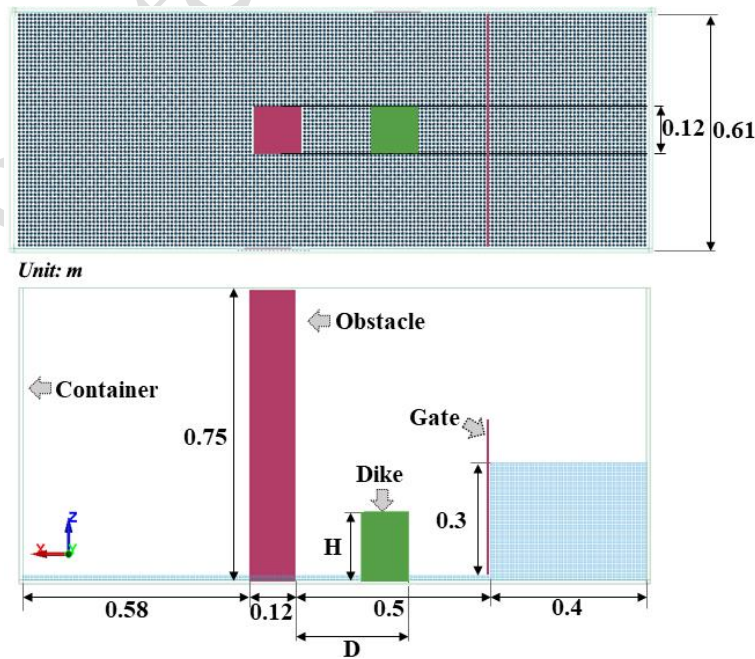


Figure 8. WSI configuration with dike

According to Figure 8, the width and thickness of the dike (0.12 m) are held constant across all simulation cases. As shown in Table 3, the dike effect is investigated for various scenarios with small and large heights (5 cm, 10 cm) and different longitudinal distances from the rigid obstacle (15 cm, 30 cm, and 45 cm) using the SPH method. Table 4 illustrates the fluid wave evolution with the dike in a three-dimensional view for different dike positions and dimensions. Figure 9 shows the time history of the force applied to the rigid obstacle for the different numerical models listed in Table 3. The maximum impact force at points A, B, and C, along with the state of fluid wave motion at the corresponding time for the small and large dikes, are shown in Figures 9-a and 9-b, respectively.

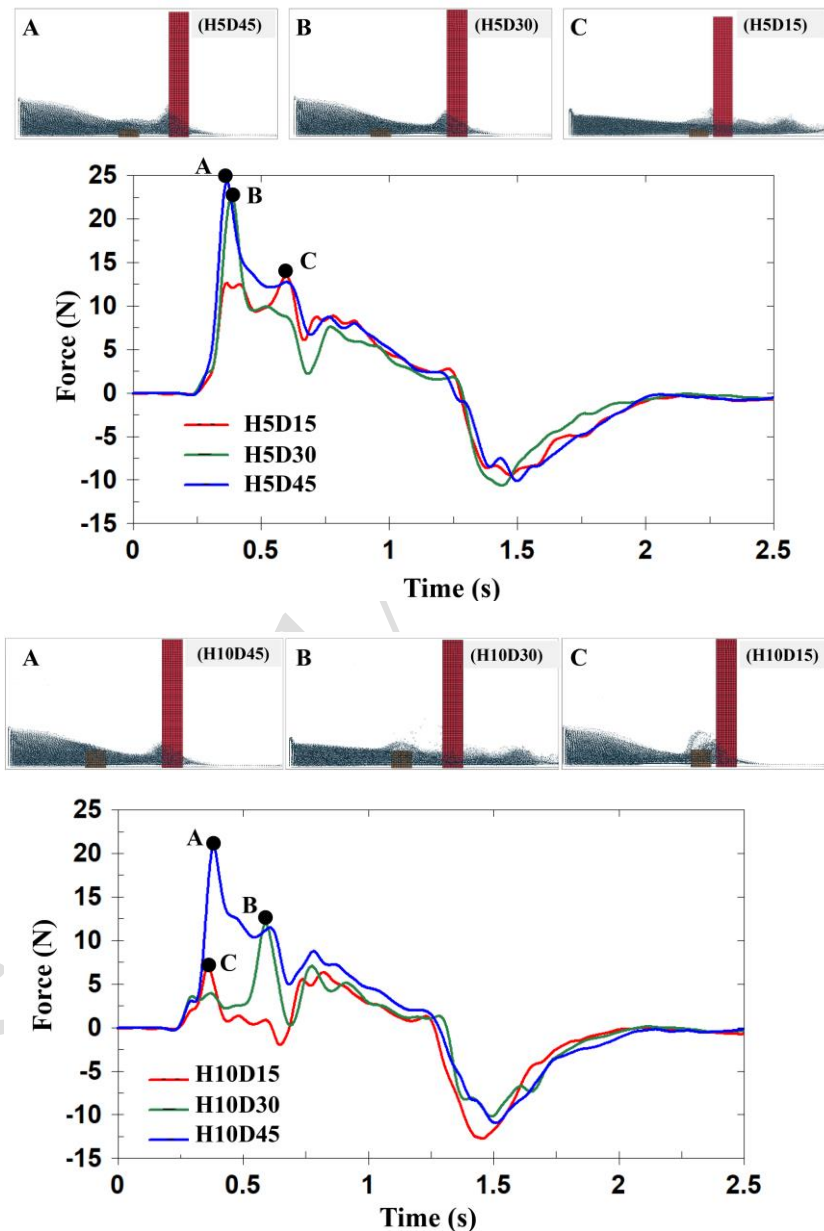


Figure 9. Fluid force on the obstacle with dike, (a) small dike, (b) tall dike

As expected, for all models, increasing the height of the dike and reducing its horizontal

distance from the obstacle results in a maximum fluid impact force less than 39.9 N (the baseline without a dike, as shown in Table 3). As demonstrated in Table 3 and Figure 9 at point "C" a comparison between H5D15 ($F_{max} = 13.4$ N) and H10D45 ($F_{max} = 7.5$ N) reveals that increasing the height of the dike (H) has a more significant effect on reducing the wave impact and maximum force compared to reducing its distance (D).

Table 4. Fluid wave evolution with dike

<i>Time/ Model</i>	<i>0.35 s</i>	<i>0.65 s</i>	<i>0.95 s</i>
H5D15			
H5D30			
H5D45			
H10D15			
H15D30			
H10D45			

As illustrated in Figure 10, the effect of incrementally enlarging the cross-section of the dike in both the longitudinal (X-direction) and transverse (Y-direction) by 0.12 m, 0.24 m, and 0.36 m is investigated.

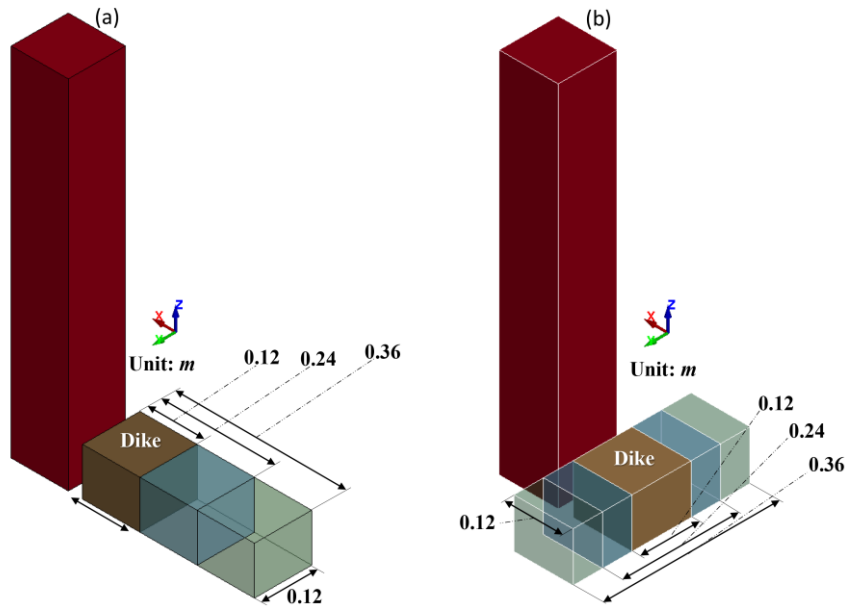
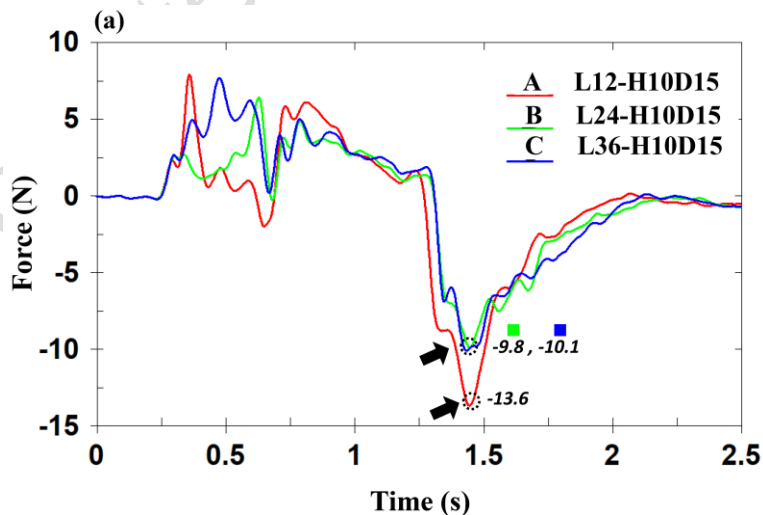


Figure 10. Dike cross sections for H10D15; (a) longitudinal, (b) transverse cross sections

As can be seen in Figure 11-a and Table 3, the longitudinal expansion (X-axis) of the dike cross-section leads to a reduction in the maximum fluid force acting on the rigid obstacle, decreasing to 9.8 N, which represents an approximate 28% reduction for the case W24-H10D15. When the cross-section is expanded in the transverse direction (Y-axis), the maximum wave-induced force decreases from 13.6 N to 9.2 N, corresponding to a reduction of approximately 33% (Figure 11-b). Therefore, modifying the cross-sectional geometry in the transverse direction has a more significant effect on mitigating the impact of hydrodynamic wave forces. These findings underscore the importance of optimizing dike geometry for wave-structure interaction (WSI) problems.



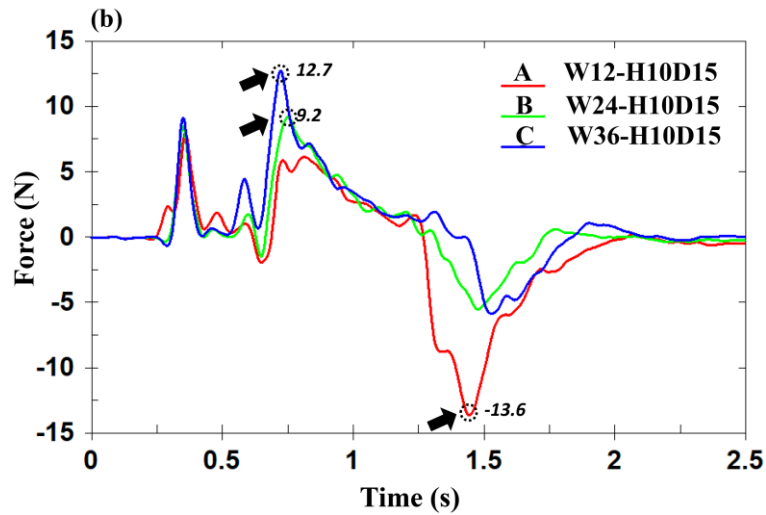


Figure 11. Fluid force with varying dike cross-sections: (a) longitudinal, (b) transverse

6. Conclusion

In this study using the LS-DYNA code, the SPH and ALE methods are utilized to simulate the impact of a large wave induced by a dam break on tall coastal structures. A clear correlation exists between the experimental and numerical values for the time history of the fluid force applied to the rigid barrier. In addition, the effect of wave reduction using a dike is analyzed for different dike heights and distances from the rigid obstacle: H: [5 cm, 10 cm] and D: [15 cm, 30 cm, 45 cm] using the SPH method. The results show that:

1. The SPH method's advantage over the ALE method is that it avoids the intensive computational cost of re-meshing. The SPH approach allows for the deactivation of failing particles during particle loop processing.
2. The SPH approach demonstrates a better fit with experimental data compared to the ALE method, particularly in capturing the minimum and maximum wave force values and fluid wave evolution. Consequently, we employ the SPH method for the parametric study.
3. SPH requires a large number of particles to solve three-dimensional problems, which increases computational cost and time.
4. We considered a 1 cm element size for the ALE model and 683,394 particles for the SPH model in the mesh convergence investigation. This approach reduced calculation time and cost while providing reliable results.
5. SPH is used to study the dike effect for small and large heights (5 cm, 10 cm) and longitudinal distances from the rigid obstacle (15 cm, 30 cm, and 45 cm). Increasing dike height and decreasing horizontal distance from the barrier reduce the maximum fluid impact force to less than 39.9 N (the baseline without a dike) for all models.
6. At point "C," a comparison between H5D15 ($F_{max} = 13.4\text{ N}$) and H10D45 ($F_{max} = 7.5\text{ N}$) indicates that increasing the height of the dike (H), as opposed to reducing its distance (D), significantly reduces the effect of the wave and the maximum force.
7. Longitudinal expansion of the dike cross-section reduces the maximum fluid force to 9.8 N (~28% decrease), while transverse expansion decreases it from 13.6 N to 9.2 N (~33% reduction). Transverse modifications more effectively mitigate hydrodynamic wave forces, highlighting the importance of optimizing dike geometry for wave-structure interaction (WSI) challenges.

Funding

This research received no external funding.

Conflicts of interest

The authors declare no conflict of interest.

Authors contribution statement

A. Rahmati Alaei: Writing – original draft, Visualization, Software, Methodology, Numerical analysis, Data curation, Conceptualization.

H. Rokhi: Offering the initial study idea, Numerical analysis, Writing – review & editing.

Acknowledgments

The authors would like to acknowledge the use of artificial intelligence (AI) tools for improving the language and readability of this paper.

References:

- Altomare, C., Scandura, P., Cáceres, I. and Viccione, G. (2023). "Large-scale wave breaking over a barred beach: SPH numerical simulation and comparison with experiments", *Coastal Engineering*, 185, 104362. <https://doi.org/10.1016/j.coastaleng.2023.104362>.
- Altomare, C., Tafuni, A., Domínguez, J.M., Crespo, A.J.C., Gironella, X. and Sospedra, J. (2020). "SPH simulations of real sea waves impacting a large-scale structure", *Journal of Marine Science and Engineering*, 8(10), 826. <https://doi.org/10.3390/jmse8100826>.
- Bai, X.-D., Zhang, W., Zheng, J.-H. and Wang, Y. (2020). "On the mass source internal wave making method for ALE based numerical wave tank", *Journal of Marine Science and Technology*, 25(4), 1093–1102. <http://dx.doi.org/10.1007/s00773-020-00702-z>.
- Basting, S., Quaini, A., Čanić, S. and Glowinski, R. (2017). "Extended ALE method for fluid–structure interaction problems with large structural displacements", *Journal of Computational Physics*, 331, 312–336. <https://doi.org/10.1016/j.jcp.2016.11.043>.
- Cai, Z., Topa, A., Djukic, L.P., Herath, M.T. and Pearce, G.M.K. (2021). "Evaluation of rigid body force in liquid sloshing problems of a partially filled tank: Traditional CFD/SPH/ALE comparative study", *Ocean Engineering*, 236, 109556. <https://doi.org/10.1016/j.oceaneng.2021.109556>.
- Chang, C.-C. and Wu, Y.-T. (2023). "SPH modeling of dam-break bores on smooth and macro-roughness slopes", *Ocean Engineering*, 279, 114484. <https://doi.org/10.1016/j.oceaneng.2023.114484>.
- Crespo, A.J.C., Domínguez, J.M., Rogers, B.D., Gómez-Gesteira, M., Longshaw, S., Canelas, R., Vacondio, R., et al. (2015). "DualSPHysics: Open-source parallel CFD solver based

- on Smoothed Particle Hydrodynamics (SPH)", *Computer Physics Communications*, 187, 204–216. <https://doi.org/10.1016/j.cpc.2014.10.004>.
- Domínguez, J.M., Crespo, A.J.C., Hall, M., Altomare, C., Wu, M., Stratigaki, V., Troch, P., et al. (2019). "SPH simulation of floating structures with moorings", *Coastal Engineering*, 153, 103560. <http://doi.org/10.1016/j.coastaleng.2019.103560>.
- Gómez-Gesteira, M., Crespo, A.J.C., Rogers, B.D., Dalrymple, R.A., Dominguez, J.M. and Barreiro, A. (2012). "SPHysics—development of a free-surface fluid solver—Part 2: Efficiency and test cases", *Computers & Geosciences*, 48, 300–307. <https://doi.org/10.1016/j.cageo.2012.02.028>.
- Han, X. and Dong, S. (2022). "Experimental investigation and SPH simulation on interaction between regular waves and vertical breakwater under medium-long period waves", *International Journal of Naval Architecture and Ocean Engineering*, 14, 100467. <https://doi.org/10.1016/j.ijnaoe.2022.100467>.
- Jacob, B., Drawert, B., Yi, T.-M. and Petzold, L. (2021). "An arbitrary Lagrangian Eulerian smoothed particle hydrodynamics (ALE-SPH) method with a boundary volume fraction formulation for fluid-structure interaction", *Engineering Analysis with Boundary Elements*, 128, 274–289. <https://doi.org/10.1016/j.enganabound.2021.04.006>
- Kelager, M. (2006). "Lagrangian fluid dynamics using smoothed particle hydrodynamics", University of Copenhagen: Department of Computer Science, 2.
- Liu, X., Xu, H., Shao, S. and Lin, P. (2013). "An improved incompressible SPH model for simulation of wave–structure interaction", *Computers & Fluids*, 71, 113–123. <https://doi.org/10.1016/j.compfluid.2012.09.024>.
- Lou, Y.-F. and Jin, X.-L. (2014). "Numerical simulation of solitary wave and drifting object interacting with breakwater using the ALE method", *Coastal Engineering Journal*, 56(03), 1450015. <http://dx.doi.org/10.1142/S0578563414500156>.
- Nishiura, D., Furuichi, M. and Sakaguchi, H. (2015). "Computational performance of a smoothed particle hydrodynamics simulation for shared-memory parallel computing", *Computer Physics Communications*, 194, 18–32. <https://doi.org/10.1016/j.cpc.2015.04.006>.
- Ozdemir, Z., Moatamedi, M., Fahjan, Y. and Souli, M. (2009). "ALE and fluid structure interaction for sloshing analysis", *The International Journal of Multiphysics*, 3(3), 307–336. <http://dx.doi.org/10.1260/175095409788922257>.
- Pozorski, J. and Olejnik, M. (2024). "Smoothed particle hydrodynamics modelling of multiphase flows: an overview", *Acta Mechanica*, 235(4), 1685–1714. <https://doi.org/10.1007/s00707-023-03763-4>.
- Ren, X., Sun, Z., Wang, X. and Liang, S. (2018). "SPH numerical modeling for the wave–thin structure interaction", *China Ocean Engineering*, 32(2), 157–168. <http://dx.doi.org/10.1007/s13344-018-0017-x>.

- Rezaiee-Pajand, M., Kazemiyan, M.S. and Mirjalili, Z. (2024). "A Novel Method for Modal Analysis of Dam-Reservoir Systems", *Civil Engineering Infrastructures Journal*, 57(1), 33–59.
- Salis, N., Hu, X., Luo, M., Reali, A. and Manenti, S. (2024). "3D SPH analysis of focused waves interacting with a floating structure", *Applied Ocean Research*, 144, 103885. <https://doi.org/10.1016/j.apor.2024.103885>.
- Sunara, M., Gotovac, B., Radnic, J. and Harapin, A. (2021). "Numerical analysis of pressures on rigid structures using the smoothed particle hydrodynamics method", *Scientia Iranica*, 28(3), 1066–1078. <https://doi.org/10.24200/sci.2020.22052>.
- Torabbeigi, M., Akbari, H., Adibzade, M. and Abolfathi, S. (2024). "Modeling wave dynamics with coastal vegetation using a smoothed particle hydrodynamics porous flow model", *Ocean Engineering*, 311, 118756. <https://doi.org/10.1016/j.oceaneng.2024.118756>
- Wang, S. and Chang, C.-W. (2025). "SPH simulations to investigate the influence of realistic mangroves in reducing breaking wave forces on coastal structures", *Ocean Engineering*, 316, 120014. <http://dx.doi.org/10.1016/j.oceaneng.2024.120014>.
- Wu, G. and Garlock, M. (2024). "Investigating the effects of box girder bridge geometry on solitary wave force using SPH modeling", *Coastal Engineering*, 187, 104430. <https://doi.org/10.1016/j.coastaleng.2023.104430>
- Wu, G., Garlock, M. and Wang, S. (2022). "A decoupled SPH-FEM analysis of hydrodynamic wave pressure on hyperbolic-paraboloid thin-shell coastal armor and corresponding structural response", *Engineering Structures*, 268, 114738. <http://dx.doi.org/10.1016/j.engstruct.2022.114738>.
- Xie, C.-M., Yang, J.-C., Sun, P.-N., Lyu, H.-G., Yu, J. and Ye, Y.-L. (2023). "An accurate and efficient HOS-meshfree CFD coupling method for simulating strong nonlinear wave–body interactions", *Ocean Engineering*, 287, 115889. <https://doi.org/10.1016/j.oceaneng.2023.115889>
- Xu, J., Wang, J. and Souli, M. (2015). "SPH and ALE formulations for sloshing tank analysis", *The International Journal of Multiphysics*, 9(3), 209–224. <https://doi.org/10.1260/1750-9548.9.3.209>.
- Yreux, E. (2018). "Fluid flow modeling with SPH in LS-DYNA®", *Proceedings of the 15th International LS-DYNA Users Conference*, Dearborn, MI, USA.